Detailed comparison of experimental and theoretical heliumlike Ti and Ca satellite line spectra emitted from a laser-produced plasma

A. Demir,[1] P. Zeitoun,[1,*] G. J. Tallents,[1] E. Fill,[2] G. Jamelot,[3] Y. L. Li,[2] M. Nantel,[3,†] G. J. Pert,[4] B. Rus,[5] and D. Schlögl[2]

[1]*Department of Physics, University of Essex, Colchester CO4 3SQ, United Kingdom*

[2]*Max-Planck Institute für Quantenoptik, 85748 Garching bei München, Germany*

[3]*Laboratoire de Spectroscopie Atomique et Ionique, Bâtiment 350, Université Paris-Sud, 91405 Orsay Cedex, France*

[4]*Department of Physics, York University, York, YO1 5DD, United Kingdom*

[5]*Department of Gas Lasers, Institute of Physics, 18040 Prague 8, Czech Republic*

(Received 22 July 1996)

Time- and space-integrated x-ray spectra of heliumlike titanium (Ti XXI) and heliumlike calcium (Ca XIX), resonance, and satellite lines emitted from a laser-produced plasma during a study of Li-like x-ray lasing have been observed with a LiF ($2d=4.027$ Å) crystal spectrometer and compared to model calculations of the spectra. We show that the emission can be accurately calculated for critical and subcritical density laser-produced plasmas assuming coronal equilibrium and that published atomic data for these satellite lines produce good agreement with the observed spectra. The He-like Ca and Ti intercombination to jkl Li-like satellites intensity ratios are proposed as useful and accurate diagnostics of electron temperatures in laser-produced plasmas for temperatures above 0.5 keV. [S1063-651X(97)09202-7]

PACS number(s): 52.25.−b, 52.50.Jm, 52.70.−m, 42.55.Vc

I. INTRODUCTION

Saturated soft x-ray lasers using neonlike ions pumped collisionally are now readily achieved [1,2]. However, the shortest wavelength produced so-far is only at 9.9 nm (in Ne-like Ag) [3]. Shorter wavelengths are of interest for future biological applications [4]. Such biological applications ideally require an X-UV laser emitting near or inside the so-called ''water window'' (2.3–4.4 nm) between the absorption edges of oxygen and carbon. Ni-like ions pumped collisionally have lased at 4.5 nm (Ta) and 3.9 nm (Au). However, more than 10 kJ optical laser pumping energy was necessary [5].

Recombination in Li-like ions has produced gain on several elements ranging from Si to Ca with a relatively low pumping energy [6–8]. A gain of about 4 cm^{-1} has been reported [7,8] for the $1s^2 3d$-$1s^2 4f$ transition in Li-like Ca at 4.7 nm with a pump laser irradiance of $\approx 2\times 10^{13}$ W/cm^2. In contrast, to achieve gain on Ni-like Ta [5], the required pumping irradiance is almost two orders of magnitude higher (10^{15} W/cm^2). These previous experiments with Li-like Ca were performed with 1 cm long plasmas. We attempted [9] to repeat the experiments of Xu *et al.* [7,8] with longer Ca targets (up to 3 cm) with the aim of achieving a gain-length product high enough ($\approx$15) to saturate the amplification in single pass. We also investigated [9] lasing on Li-like Ti as the $1s^2 3d$-$1s^2 5f$ transition has a better wavelength for biological applications (3.2 nm). These studies of x-ray laser output will be reported elsewhere [9], but in summary, we observed no gain on Li-like Ti and only weak gain (0.7 cm^{-1}) on Ca, partly at least because as we shall show in this paper, the electron temperatures produced were not high enough to produce a sufficiently large population of He-like ions which could subsequently recombine to create Li-like population inversions.

Modeling studies [9] show that lasing on Li-like recombination schemes requires a control of the plasma history during the heating-ionization phase as well as the later cooling recombination phase. The heating has to be sufficient to achieve a dominantly He-like plasma by the end of the pump laser pulse. Furthermore, the heating phase has to be short enough to produce a high-density plasma which will expand quickly and give a strong adiabatic cooling. The He→Li collisional recombination rate depends on N_e^3/T_e^2, where N_e and T_e are the electron density and temperature respectively and so this value must be high enough to produce population inversions once the plasma starts to expand adiabatically with N_e^2/T_e^3 approximately constant [10]. Previous work has shown the deleterious effect on the amplification of pump laser inhomogeneities [11]. Consequently, during this experiment, it was crucial to accurately diagnose the Ca and Ti plasma He- and Li-like stages along the plasma line.

Dielectronic and other satellites lines [12–16] are important features of x-ray spectra from highly charged ions in laboratory and astrophysical plasma and the intensities of hydrogenlike to lithiumlike satellites are often used to diagnose plasma conditions [17–19]. Satellite lines are particularly suited for diagnostic applications as the lines are usually optically thin and are close together. Fewer problems of relative calibration of spectrometer and detector occur with such closely spaced lines and smaller detectors such as CCD arrays can be used. The atomic physics controlling the emission intensities of H-like to Li-like ions is also, in general, well known [20–25].

For this paper, we have recorded He-like resonance and

*Present address: Laboratoire de Spectroscopie Atomique et Ionique, Bât. 350, Université Paris-Sud, 91405 Orsay Cedex, France.

†Present address: The Center for Ultrafast Optical Science, University of Michigan, 1006 IST Building, 2200 Bonisteel Blvd., Ann Arbor, MI 48109-2099.

satellite emission from a line focused laser-produced Ti plasma (between 2.60 and 2.66 Å wavelength) and a similar Ca plasma (between 3.17 and 3.22 Å) during the above-mentioned study to observe Li-like x-ray lasing [9]. H-like and He-like emission from medium Z ions [26–33] have been previously observed. We show that the emission can be accurately calculated for the laser produced plasmas with a relatively straight forward coronal model and that published atomic data for the satellite lines produce good agreement with the observed spectra. The He-like Ca and Ti satellite spectra are thus proposed as useful diagnostics of electron temperatures in laser produced plasmas for temperatures above 0.5 keV. We will show that the principal advantages in using medium atomic number elements such as Ca and Ti is that the spectra can often be calculated assuming coronal equilibrium. Moreover, the times t_{ss} for medium atomic number elements for a steady state to be achieved are shorter and the satellite spectra are relatively more intense compared to the resonance lines which makes electron temperature measurements based on these satellite intensity ratios more accurate.

II. EXPERIMENTAL METHOD

The experiment was undertaken using the iodine laser facility [34] ASTERIX IV of the Max-Planck Institut für Quantenoptik in Garching, Germany, The 1.315 μm wavelength laser was focused to a 30 mm long by 100 μm wide line onto Ti and CaF_2 massive slab targets of between 10 mm and 25 mm length. The laser energy was between 600 and 700 J in pulses of 450 ps duration. The focusing lens consisted of six cylindrical sections, each of which focused the beam to a 3 cm long by 30–50 μm wide line focus. The overlap of the six foci results in a 100 μm wide line focus with irradiance $\cong 3\times10^{13}$ W/cm^2.

To measure the uniformity and ionization of the line focus plasma, a LiF flat crystal spectrometer ($2d=4.027$ Å) was placed at an angle of 40° to the incident laser beam in the plane of the beam and line focus with the distance between the target and crystal $\cong$150 mm. We placed a 120 μm wide vertical slit in front of the crystal to spatially resolve the plasma emission along the line focus. The diffracted x rays were detected using a 16-bit CCD system. The distance between the center of the crystal and the CCD was 60 mm. The achieved spatial resolution and resolving power ($\lambda/\Delta\lambda$) were 240 μm and 1000 respectively. A 12 μm thick Be filter was placed at the vertical slit to stop visible light from exposing the CCD detector. To record the He-like resonance line and satellite emission from Ti and Ca plasmas, the crystal was aligned to Bragg angles of 39° and 54° respectively.

Examples of the experimental time-integrated spectra of Ti and Ca are shown in Figs. 1 and 2, respectively. The He-like resonance ($1s^2\ ^1S$-$1s2p\ ^1P$), intercombination ($1s^2\ ^1S$-$1s2p\ ^3P$), forbidden lines ($1s^2\ ^1S$-$1s2p\ ^3S$), and $n=2,3,4,\ldots$ dielectronic satellite lines are observed. The lines in Figs. 1 and 2 are identified according to Gabriel's notation [12]. Most of the experimental spectral features are blends of several lines (Figs. 1 and 2).

III. DESCRIPTION OF PLASMA EMISSION MODELS

FLY [35] is a widely available quasi-steady-state collisional radiative code which is accurate for modeling and analyzing Li- to H-like K-shell spectra of elements from carbon to iron. The code evaluates the important populating and depopulating atomic processes between all Li-like quantum states up to principal quantum number $n=5$ with a hydrogen-like approximation for $n>5$ and between all $n=2$ states with a manifold average for the $n>2$ states for helium-like ions. Electron-impact excitation and ionization, three-body recombination, autoionization out of and electron capture into doubly excited states and radiative recombination are considered. The quantum number densities are calculated up to the continuum lowering limit or the state with Rydberg radius equal to the Debye length [35]. The effects of opacity on the population densities can be approximated

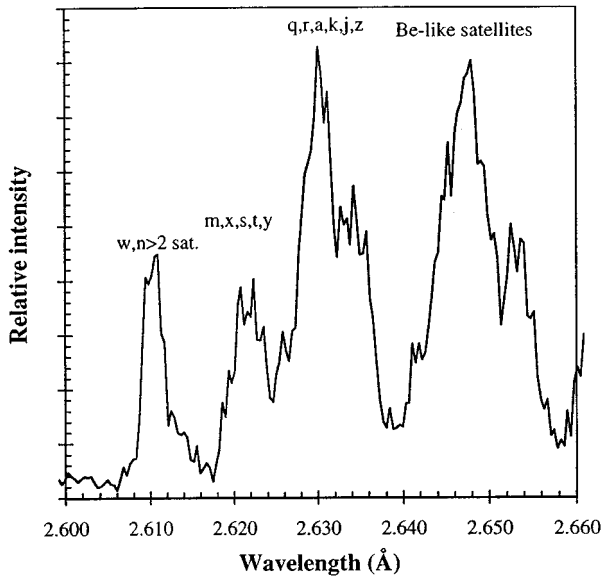

FIG. 1. Time- and space-integrated experimental He-like Ti spectrum. The spectral lines are identified following the notation of Gabriel [12].

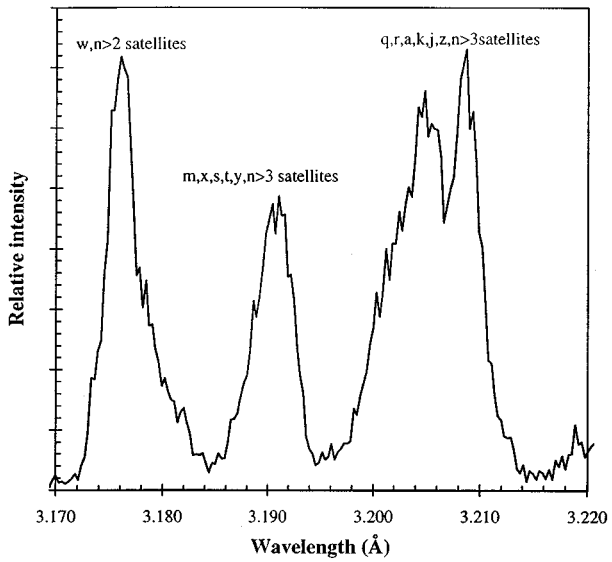

FIG. 2. Time- and space-integrated experimental He-like Ca spectrum. The spectral lines are identified following the notation of Gabriel [12].

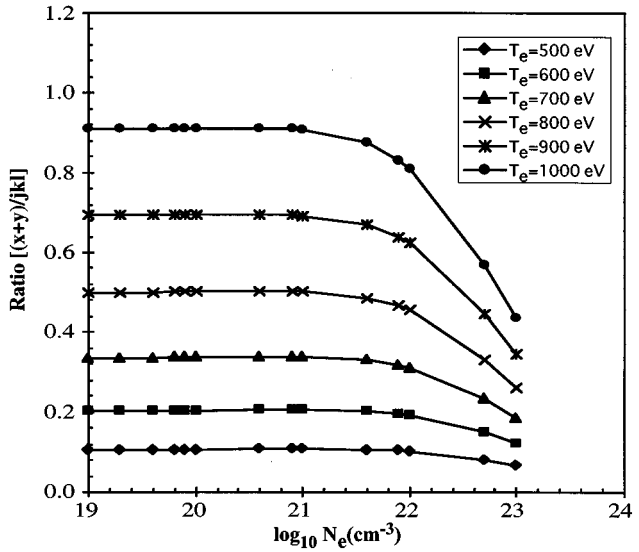

FIG. 3. The intensity ratio of the He-like intercombination lines (x,y) to jkl satellite lines of Ti as a function of electron density at different electron temperatures as calculated by the FLY code.

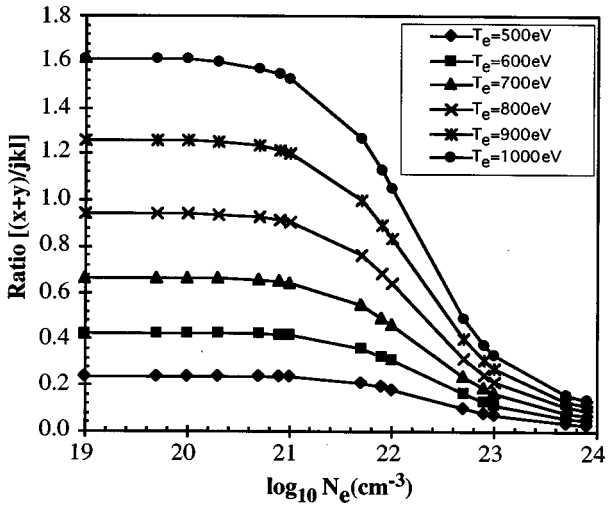

FIG. 4. The intensity ratio of the He-like intercombination lines (x,y) to jkl satellite lines of Ca as a function of electron density at different electron temperatures as calculated by the FLY code.

by an escape factor calculation. Line intensity ratios are obtained from the calculated level populations. The code also calculates microfield distributions and the profiles of the spectral lines.

In the coronal model [36] of plasma emissivity, it is assumed that exciting transitions are collisional and that all de-exciting transitions are radiative. The probability for an excited state to be depopulated by a spontaneous radiative transition is independent of density and so, if the electron density is sufficiently low, the probability of collisional de-excitation (which is proportional to electron density) becomes negligible compared with spontaneous emission. Coronal equilibrium will thus always apply for sufficiently low electron densities. As spectral line intensities depend only on the collisional excitation rates in coronal equilibrium, the intensity ratios of spectral lines are independent of the electron density.

The intensity ratios of the intercombination lines to jkl satellite lines for Ti and Ca have been calculated using the FLY code assuming steady state equilibrium (Figs. 3 and 4). These intensity ratios are constant up to electron density $\cong 1\times10^{21}$ cm^{-3} which indicates that coronal equilibrium for these $n=2$ states applies up to this density. Our hydrodynamic code modeling (discussed below in Sec. IV) shows that the line emission in our experiment is emitted largely from a region close to the critical density of the 1.3 μm laser ($\sim 6\times10^{20}$ electrons/cm^3). When coronal equilibrium applies, the upper quantum states of the He-like lines can be assumed to be populated by two mechanisms; collisional excitation from the He-like ground state and collisional inner-shell excitation from the Li-like ground state.

The intensity (photons/cm^3 s) of the He-like resonance line, intercombination line and forbidden line in coronal equilibrium is given by,

$$I = N_e N_{\mathrm{He}} C \tag{1}$$

where N_e is the electron density (cm^{-3}), N_{He} is the He-like ground state density (cm^{-3}), and C is the collisional excitation rate (cm^3 s^{-1}) from the He-like ground state. We have used the values of C calculated by the FLY code. Allowance for inner-shell excitation from Li-like ions is included in the FLY calculations.

The intensity of $n \geqslant 2$ dielectronic satellite lines is given by

$$I = N_e N_{\mathrm{He}} \left(\frac{2\pi\hbar^2}{m k_B T_e} \right)^{3/2} \exp(-E_s/k_B T_e) F_2(sf) \tag{2}$$

where T_e is the electron temperature, E_s is the energy of the upper quantum state with respect to the He-like ground state, and m, k_B, h are electron mass, Boltzmann's constant and Planck's constant respectively. $F_2(sf)$ is a function of the atomic parameters of the satellite line and is given by

$$F_2(sf) = \frac{g_s A_r^{sf}}{\Sigma_{k<s} A_r^{sk} + A_a^s} \tag{3}$$

where A_a^s and A_r^{sf} are the autoionization and radiative transition probabilities in s^{-1} and g_s is the statistical weight of the satellite level. The summation gives the net transition probability to all levels of energy less than s. The quantity $F_2(sf)$ is a branching ratio of the relevant line emission probability to the total de-excitation probability considering the two possible routes of electrons in the doubly excited s satellite state. A doubly excited ion can either re-ionize (autoionization) or one of the electrons can de-excite radiatively resulting in recombination. We have used A_a^s, A_r^{sf} and A_r^{sk} data tabulated by Bely-Dubau *et al.* [32] for Ti and by Bely-Dubau *et al.* [37] for Ca.

The q satellite line is in addition populated partly by inner-shell excitation from the Li-like ground state. The intensity due to this populating mechanism is given by

$$I = N_e N_{\mathrm{Li}} C_q \tag{4}$$

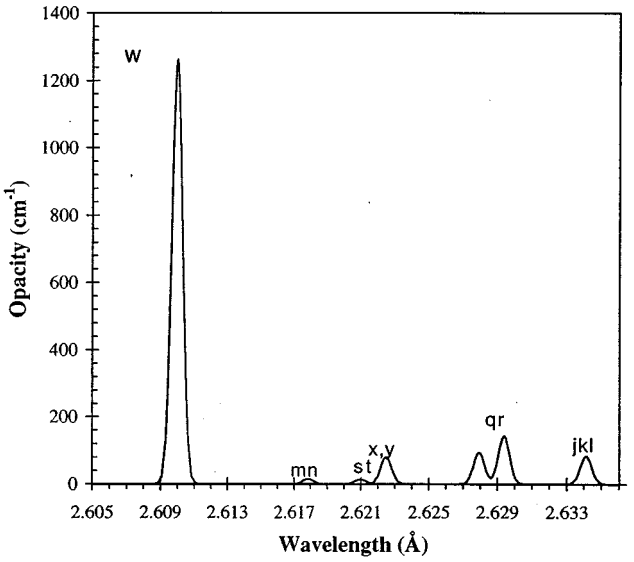

FIG. 5. The opacity of resonance line (w), intercombination (x,y) and Li-like satellite (j,k,l) lines of Ti at an electron temperature of 600 eV and electron density of 6.5×10^{20} cm^{-3} as calculated by the FLY code.

where N_{Li} (cm^{-3}) is the Li-like ground density and C_q is the collision excitation rate (cm^3 s^{-1}). The value of C_q which we have used is that calculated by Bely-Dubau *et al.* [32] for Ti and by Bely-Dubau *et al.* [37] for Ca.

The intensity of Be-like satellite lines is given by

$$I=N_eN_{\mathrm{Li}}\left(\frac{2\pi\hbar^2}{mk_BT_e}\right)^{3/2}\exp(-E_s/k_BT_e)F_2(sf) \qquad (5)$$

where the $F_2(sf)$ data are evaluated according to Eq. (3) for Ti using the atomic data of Bitter *et al.* [33].

The E_s values used in Eqs. (2) and (5) were calculated according to $E_s=E_R-E_{\mathrm{line}}$ where E_R is the ionization energy of the He-like ground state and E_{line} is the energy of the upper quantum state of the doubly excited Li- or Be-like ion. Since the wavelengths of same group satellite lines are very close together, the values of E_s are taken as 3311 eV and 4141 eV for all $n=2$ and $n=3$ dielectronic lines respectively for Ti. The E_s values are taken as 2734 eV, 3419 eV and 3615 eV for the $n=2$, $n=3$ and $n=4$ dielectronic satellite lines respectively for Ca. Grouping all satellite levels of the same spectator electron principle quantum number together produces intensity errors of at most 5% at typical temperatures ($\approx$700 eV) in the evaluation of Eqs. (2) and (5).

The 1.5D hydrodynamic and atomic physics code EHYBRID [38] was used to simulate the plasma expansion for our experiment. In the simulation a 450 ps trapezoidal, 500 J laser beam irradiates a Ti slab target so that the intensity on the target is 2×10^{13} W/cm^2. The He-like and Li-like ground state densities were taken as output from EHYBRID and were input into a postprocessor code which used Eqs. (1)–(5) to calculate the time and space averaged He-like resonance and satellite line emissions.

Opacity only affects the resonance line intensities since the oscillator strengths of the resonance lines is much larger than for other lines (for example, see Fig. 5). The effect of opacity on the resonance lines is taken into account in the modeling by an approximate solution of the equation of radiative transfer. The equation of radiative transfer can be written as

$$I_{\mathrm{tot}}=\int_{-\infty}^{\infty}\int_0^{\infty}\varepsilon(x)\Phi(\lambda)\exp\left[-\int_x^{\infty}\frac{\kappa(x)}{\cos(\phi)}\frac{\Phi(\lambda)}{\Phi(0)}dx\right]dx\,d\lambda \qquad (6)$$

where I_{tot} is the intensity escaping the plasma, $\varepsilon(x)$ is the emissivity, $\kappa(x)$ is the absorption coefficient at the center of the emission line, $\phi\approx40°$ is the angle of the spectrometer observation to the target normal and Φ is a line shape function. The inner integration is over all space x in the plasma and the outer integral is over the wavelength λ of the spectral line from line center. We assume that the line profile is Gaussian and that the emissivity $\varepsilon(x)$ and absorption coefficient $\kappa(x)$ profiles rise as a step function at $x=0$ and then decrease exponentially with x (following the electron temperature rise close to the target surface and then the exponential decrease of electron density with distance from the target). The exponential in Eq. (6) can then be expanded as a Taylor series and we can integrate each term to get

$$I_{\mathrm{tot}}=I_{\mathrm{peak}}\left(1-\frac{\tau}{(2)^{3/2}}+\frac{\tau^2}{2!(3)^{3/2}}+\frac{\tau^3}{3!(4)^{3/2}}+\cdots+\frac{(-1)^n\tau^n}{n!(n+1)^{3/2}}+\cdots\right) \qquad (7)$$

where I_{peak} is the intensity neglecting absorption and τ is the optical thickness of the plasma given by

$$\tau=\int_0^{\infty}\frac{\kappa(x)}{\cos(\phi)}dx. \qquad (8)$$

Various authors [39] have derived a similar expression as Eq. (7) for Gaussian distributions (rather than exponential) of $\varepsilon(x)$, $\kappa(x)$. Equation (7) neglects Doppler decoupling [40] which will reduce the effect of opacity by a small amount. We estimate from EHYBRID velocities that Doppler decoupling could reduce the maximum optical depths from typically $\tau\approx2$ to $\tau\approx1.5$ resulting in a maximum error in the intensity of the w line of 20%. This error in the intensities around the w line would be at least partly offset by our neglect of the absorption of satellite emission by the w transition. Our postprocessor code uses Eq. (7) to allow for opacity on the He-like w line using the values of τ calculated from the electron density and temperature output of EHYBRID and the FLY determined opacity (e.g., Fig. 5) at each timestep.

The measured experimental FWHM of the He-like resonance line is 2 mÅ. A broadening of 1 mÅ is predicted because of Doppler and Stark broadening by the FLY code. However, most of the broadening is due to the instrumental effects because of the plasma size (a width of 200 μm). We have assumed that all of the lines have a width of 2 mÅ FWHM in our modeling.

IV. RESULTS

Spectra of titanium calculated assuming coronal equilibrium as outlined above [Eqs. (1)–(5)] for single electron

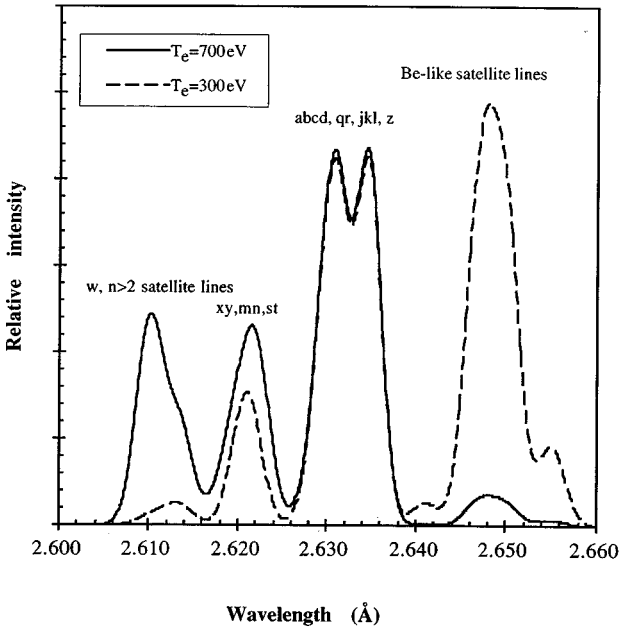

FIG. 6. The theoretical spectrum of Ti at different electron temperatures (300 eV and 700 eV) as calculated by our postprocessor code.

temperatures are shown in Fig. 6. At low T_e (300 eV), the Be-like satellite lines are stronger than the other lines and the He-like resonance line is weak. When T_e increases (700 eV), the Be-like satellite lines become weak and the He-like resonance line intensities increase. It is necessary to integrate the theoretical spectrum in time and space using the predicted time and space variation of N_e and T_e from EHYBRID to obtain a comprehensive agreement with the experimental spectra (Fig. 7). During the laser heating the peak temperature was ≈700 eV (Fig. 8), while at later times the electron temperature drops due to adiabatic plasma expansion and the emission is dominated by strong Be-like satellite emission. The agreement between the Fig. 7 theoretical and experimental spectra is good apart from the j satellite line intensity which appears ≈40% less intense experimentally than the post-processor code calculates and the Be-like satellites at 2.641 Å and 2.655 Å which are experimentally 2–4 times more intense than calculated.

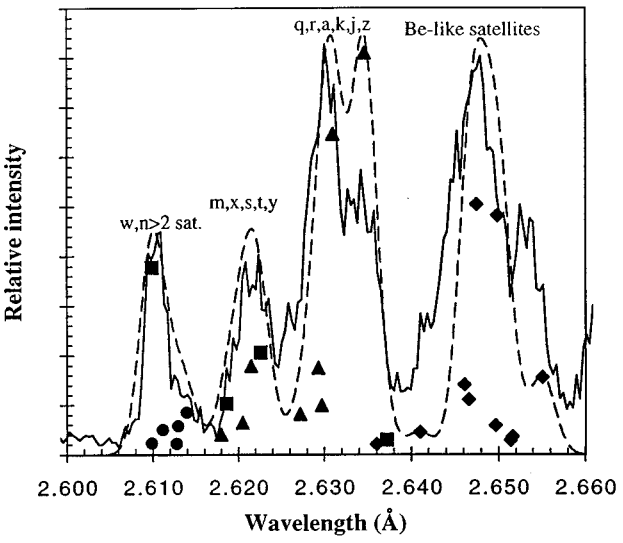

FIG. 7. Time- and space-integrated experimental (solid line) and post-processor (dashed line) He-like Ti spectrum. Theoretical positions and relative intensities (see text) of all the individual spectral lines considered are also shown. Here ● shows $n=3$ satellite lines, ▲ represents $n=2$ (m,s,t,q,r,a,k,j) satellites, ■ shows the (w,x,y,z) lines and ◆ shows Be-like satellite lines.

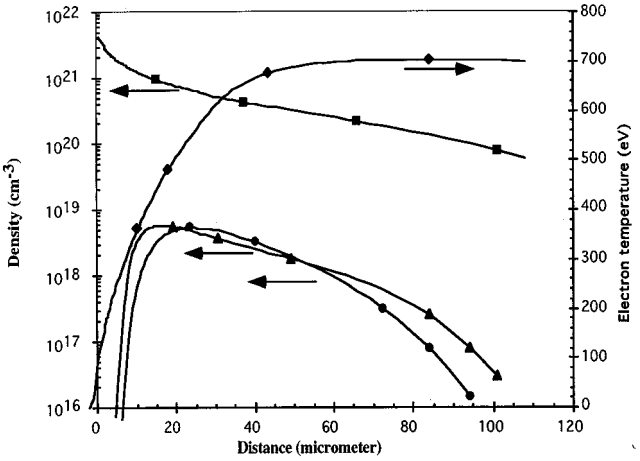

FIG. 8. The output of EHYBRID at the peak irradiance from the laser. The symbols designate ● the He-like ground state density, ▲ the Li-like ground state density, ■ the electron density and ◆ the electron temperature of Ti as a function of distance.

Figure 9(a) shows the ratios of intercombination (x,y) plus Li-like m,n,s,t satellite lines to Li-like j,k,l,q,r,a,b,c,d satellite plus forbidden (z) line of Ti calculated using both FLY and our post-processor code. The agreement between the code results is excellent at higher temperatures, but less so at lower temperatures, where our calculation involving a larger number of spectral lines is more accurate. The electron temperature obtained from the experimental line ratio and the postprocessor calculation is ≈500–700 eV [Fig. 9(b)] in agreement with the EHYBRID calculated peak electron temperatures at the critical density (see, e.g., Fig. 8). The error bars on the line focus axis show the spatial resolution of the spectrometer. The errors on the temperature measurements reflect the accuracies of measuring the line ratios. Our poor modeling of the j satellite line intensity could, in addition, introduce a systematic electron temperature error making our deduced temperatures up to an estimated ≈50 eV too high.

To simulate the Ca spectrum, He-like and Li-like ground state densities, resonance (w), intercombination (x,y) and forbidden (z) line intensities for a single electron temperature calculated by FLY were used, but with the calculation of the $n\geqslant 2$ spectator electron satellite line intensities using the data published by Bely-Dubau *et al.* [37]. Since all the Ca lines are populated from the He-like ground state level (see Sec. III), a single temperature calculation is sufficiently accurate for the Ca spectrum. The calculated theoretical spectrum for a temperature of 730 eV is shown in Fig. 10 superimposed on the experimental spectrum. The effect of $n\geqslant 3$ dielectric satellite lines on the He-like resonance line is simulated well. Overall the single temperature theoretical

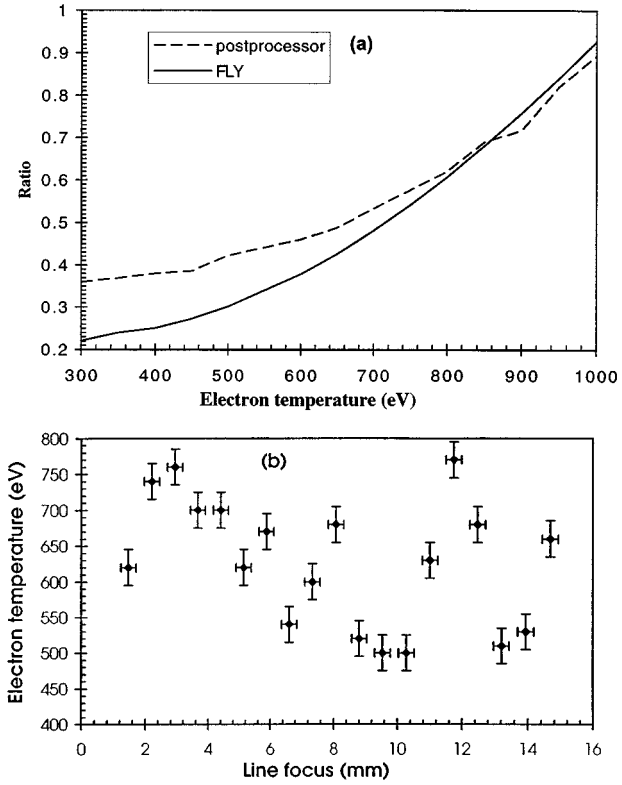

FIG. 9. (a) The intensity ratio of the intercombination (x,y) plus Li-like m,n,s,t to the Li-like j,k,l,q,r,a,b,c,d satellites plus forbidden (z) lines of Ti plasma as a function of electron temperature. The solid line is calculated by the FLY code, while the dashed line is calculated by our post-processor code. The effects of $n \geqslant 3$ satellites lines were included in the post-processor calculations. (b) The electron temperature of the Ti plasma along the line focus deduced using the post-processor ratio.

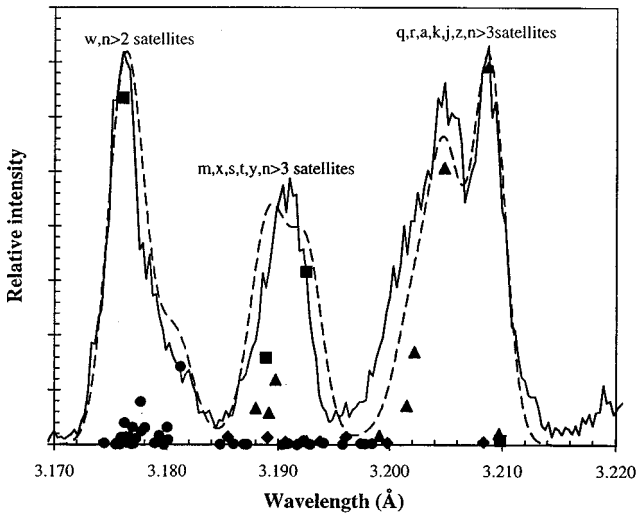

FIG. 10. Time- and space-integrated experimental (solid line) and single temperature (730 eV) post-processor (dashed line) He-like Ca spectrum. Theoretical positions and relative intensities (see text) of all the individual spectral lines considered are also shown. Here ● shows $n=3$ satellite lines, ▲ represents $n=2$ (m,s,t,q,r,a,k,j) satellites, ■ shows the (w,x,y,z) lines and ◆ designates $n=4$ Li-like satellite lines.

spectrum (not time- and space-integrated) for Ca fits the experimental spectrum well.

Figure 11(a) shows the ratio of intercombination (x,y) plus Li-like m,n,s,t satellites lines to Li-like j,k,l,q,r,a,b,c,d satellites plus forbidden (z) lines of Ca calculated using both FLY and our post-processor code. The electron temperature obtained from the experimental line ratios is $\approx$700–800 eV [Fig. 11(b)]. There is a slight difference between the FLY and post-processor calculations because of the inclusion of the $n \geqslant 3$ satellites and small differences in the atomic data for the $n=2$ satellites in our calculations.

V. DISCUSSION

Lower atomic number elements such as Al or NaF have been used as tracer or diagnostics layers by various authors [41–43]. In this section, we will discuss the use of medium Z elements $(Z=17-26)$ for laser produced plasma diagnostics. Figure 12 shows the maximum electron density as a function of nuclear charge Z for coronal equilibrium to apply. This maximum density was deduced using FLY and is the density where the intercombination (x,y) lines and j,k,l dielectronic satellite line ratios start to change with increasing electron density at an electron temperature of 500 eV. This maximum electron density scales as $Z^{5.5}$. The electron densities for $Z \geqslant 20$ is greater than 1×10^{21} cm^{-3} which is above or close to the critical density (where emission peaks) of 1 μm or higher wavelength lasers.

Figure 13 shows the intensity ratio of the Li-like dielectronic satellite (a,b,c,d,q,r,j,k,l) lines to the He-like intercombination lines (x,y) plus the Li-like dielectronic satellite (m,n,s,t) lines and the intensity ratio of the Li-like dielectronic satellite (a,b,c,d,q,r,j,k,l) lines to the He alpha resonance line (w) as a function of nuclear charge Z at the maximum electron density for coronal equilibrium and at of an electron temperature of 600 eV. The line ratios show similar behavior at other temperatures. The intensity of the Li-like satellite lines increase with Z as approximately Z^5 relative to the He-like intercombination lines (x,y). The summed experimental intensity ratios of the Li-like satellite (a,b,c,d,q,r,j,k,l) lines to the x,y plus the Li-like satellite (m,n,s,t) lines plus the for Ca and Ti are also shown on Fig. 13 and are in approximate agreement with the theoretical values. There is a small discrepancy between the theoretical and experimental results of the line ratios of the Li-like satellite (a,b,c,d,q,r,j,k,l) lines to the He-like resonance line (w) because of the effect of opacity on the experimental resonance line (w) which is not considered in the theory calculation for Fig. 13.

Gabriel [12] suggested in his original paper on satellite lines that the He-like resonance line and Li-like satellites lines would be useful as temperature diagnostics. However, for laser produced plasmas, the He-like resonance line intensity is not very useful because the line is usually affected by opacity (see Fig. 5). However, intercombination lines which are produced by the same populating mechanism as resonance lines and for higher Z elements are as intense (see Fig. 13) and are optically thin (see Fig. 5). For this reason, we have used the ratio of the intercombination and other satellite lines for our temperature diagnostics.

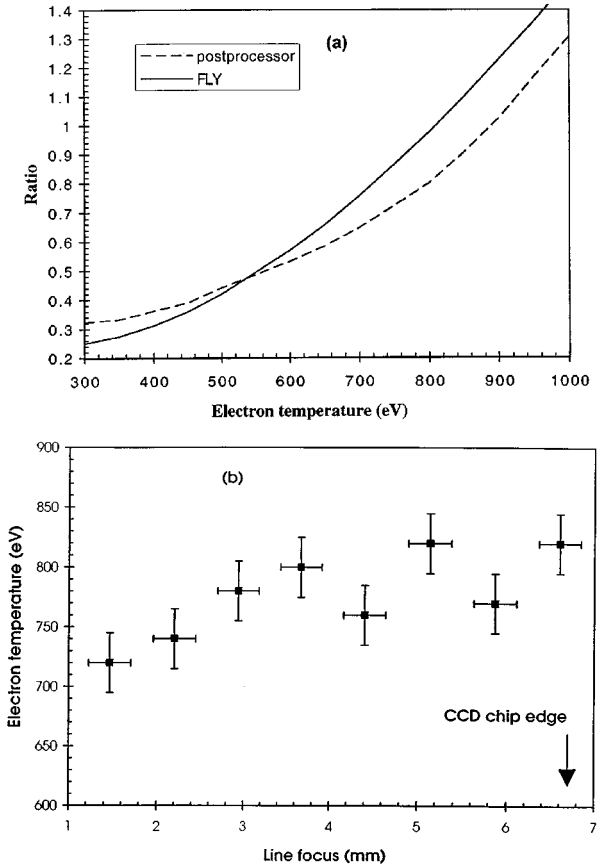

FIG. 11. (a) The intensity ratio of the intercombination (x,y) plus Li-like m,n,s,t to Li-like j,k,l,q,r,a,b,c,d satellites plus forbidden (z) lines of a Ca plasma. The solid line is calculated by the FLY, code while the dashed line is calculated by our post-processor code. The effects of $n \geqslant 3$ satellites lines were included in the post-processor calculations. (b) The electron temperature of the Ca plasma along the line focus deduced using the post-processor ratio. Only part of the line focus was observed on the spectrometer. The detector spatial limit is indicated.

We have undertaken both the FLY and our post-processor calculations of intensities assuming steady-state equilibrium. Figure 14 shows the relaxation time to steady state of the relative intensities of He-like resonance, intercombination and satellite lines as a function of nuclear charge Z. This plot was obtained from the relaxation time of the He-like resonance and jkl satellites lines ratios and the intercombination to jkl lines ratio calculated using FLY in time-dependent mode. An initial steady state calculation of ionization balance for a low electron temperature (200 eV) was allowed to relax to the ionization and emission at the indicated (Fig. 14) temperature of 500 eV. The time for this to occur was taken as the relaxation time. The relaxation times scale as Z^{-8}. The relaxation time obtained from the He-like intercombination (x,y) to jkl satellite line ratio is longer than the He-like resonance (w) to jkl satellite line ratio because the upper state of the intercombination line is metastable. Steady state calculations can be used with laser-produced plasma provided the laser pulse lengths are significantly (say a factor 10) longer than the plotted relaxation times. This implies that steady state calculations of He-like line intensities can be used as diagnostics with short pulse (0.1–1 ps) laser plasmas

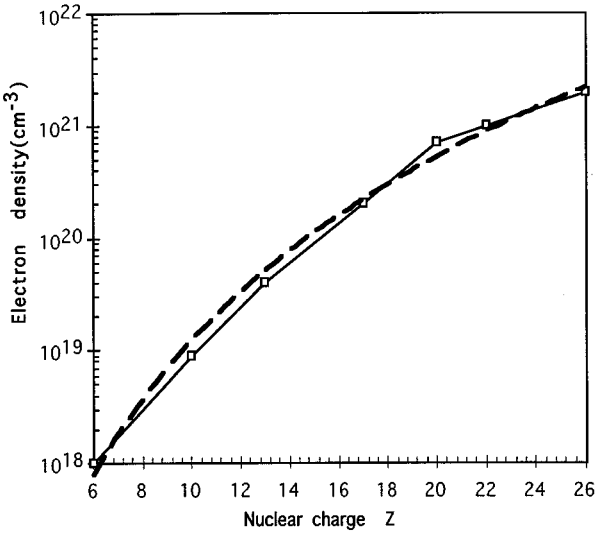

FIG. 12. The maximum electron density as a function of nuclear charge Z for coronal equilibrium to apply at an electron temperature of 500 eV. A fit of the form $N_e \propto Z^{5.5}$ to the FLY calculated data is shown as a broken line.

provided $Z > 20$ (Fig. 14). However, in sub-ps interactions with solid targets, coronal equilibrium will not apply in the initial approximately solid density plasmas formed (see Fig. 12).

VI. CONCLUSION

Time- and space-integrated x-ray spectra of helium-like titanium (Ti XXI) and helium-like calcium, Ca XIX, resonance and satellite lines emitted from a laser-produced plasma have been observed and compared to model calculations of the

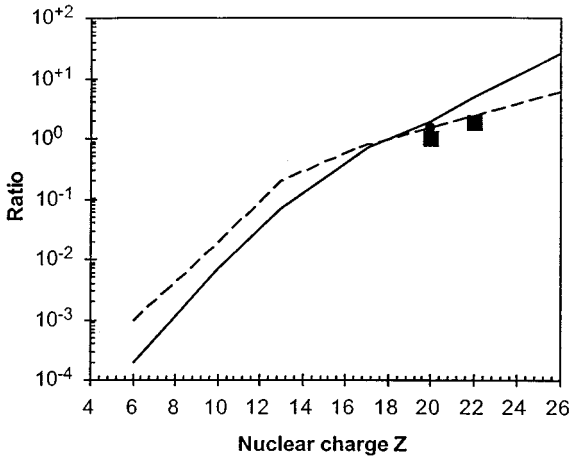

FIG. 13. The ratio of the Li-like dielectronic satellite (a,b,c,d,q,r,j,k,l) lines to the He-like resonance line (w) (solid line) and the He-like intercombination lines (x,y) plus the Li-like dielectronic satellite (m,n,s,t) lines (dashed line) as a function of nuclear charge Z at an electron temperature of 600 eV and below the maximum electron density for coronal equilibrium as calculated using the FLY code. Experimental data points for Ca and Ti are also shown (■ shows the ratio to the w lines and ● to the x,y,m,n,s,t lines).

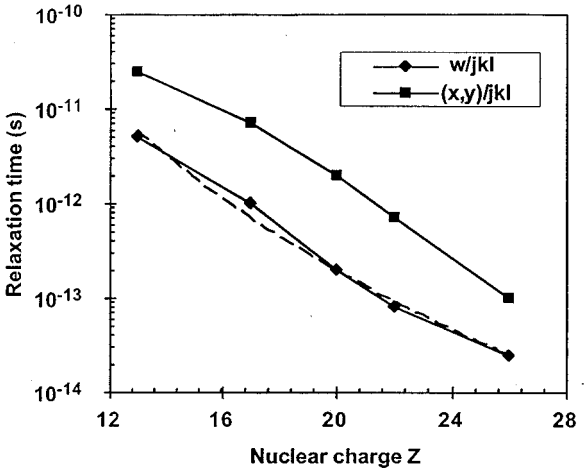

FIG. 14. Relaxation times t_{ss} to achieve steady state equilibrium as calculated by FLY as a function of nuclear charge Z for an electron temperature of 500 eV and electron density of 6×10^{20} cm^{-3}. A fit of the form $t_{ss}\propto Z^{-8}$ is shown as a broken line. The plots show the time to reach steady-state values for the resonance (w) and intercombination (x,y) to jkl satellite line intensity ratios as labeled.

spectra. We have shown that the emission can be accurately calculated for laser-produced plasmas assuming coronal equilibrium and that published atomic data for these satellite lines can produce good agreement with the observed spectra. The He-like Ca and Ti intercombination to jkl Li-like satellites have been proposed as useful and accurate diagnostics of electron temperatures in laser produced plasmas for temperatures above 0.5 keV since these lines have low opacity. Using the intercombination to jkl relative intensities, we have determined the electron temperature along the plasma lines used to investigate Li-like x-ray lasing in Ca and Ti. For Ti, we have observed an average T_e along the line focus of 600 eV with ±100 eV variations. Such a plasma was not sufficiently hot or homogeneous to achieve a good amplification of the $3d$-$4f$ and $3d$-$5f$ Li-like lines. The Ca plasma was hotter and more uniform with an average T_e of 750 eV and only ±50 eV variations and showed a small gain.

The principal advantage in using higher atomic number elements such as Ca and Ti is that in sub-critical plasmas the spectra can be calculated assuming coronal equilibrium (the maximum density for coronal equilibrium $N_{\max}\propto Z^{5.5}$), the times t_{ss} for a steady state to be achieved are shorter ($t_{ss}\propto Z^{-8}$) and the satellite spectra are relatively more intense compared to the resonance lines which makes electron temperature measurements based on these satellite intensity ratios more accurate.

ACKNOWLEDGMENTS

The authors gratefully acknowledge the technical and operational support given by the staff of ASTERIX IV laser team at Max-Planck Institut für Quantenoptik. This work was supported by the European Union Large Scale Facilities and Scientific Network Programmes and by the Commission of the European Communities in the framework of the Association Euratom–Max Planck-Institut für Plasmaphysik.

[1] D. L. Matthews, P. L. Hagelstein, M. D. Rosen, M. J. Eckart, N. M. Ceglio, A. U. Hazi, H. Medecki, B. J. MacGowan, J. E. Trebes, B. L. Whitten, E. M. Compbell, C. W. Hatcber, A. M. Hawrylunk, R. L. Kauffman, L. D. Pleasance, G. Rambach, J. H. Scofield, G. Stone, and T. A. Weaver, Phys. Rev. Lett. **54**, 110 (1985).

[2] A. Carillon, H. Z. Chen, P. Dhez, L. Dwivedi, J. Jacoby, P. Jaeglé, G. Jamelot, J. Zhang, M. H. Key, A. Kidd, A. Klisnick, R. Kodama, J. Krishnam, C. L. S. Lewis, P. Norreys, D. O'Neill, G. J. Pert, S. A. Ramsden, J. P. Raucourt, G. J. Tallents, and J. Uhomoibhi, Phys. Rev. Lett. **68**, 2917 (1992).

[3] D. Desenne, L. Berthet, J. L. Bourgade, J. Bruneau, A. Carillon, A. Decoster, A. Dulieu, H. Dumont, S. Jacquemot, P. Jaeglé, G. Jamelot, M. Louis-Jacquet, J. P. Raucourt, C. Reverdin, J. P. Thébault, and G. Thiell, Inst. Phys. Conf. Ser. No. **116**, 351 (1990).

[4] R. A. London, M. D. Rosen, and J. E. Trebes, Appl. Opt. **28**, 3397 (1989).

[5] B. J. MacGowan, L. B. Da Silva, D. J. Fields, A. R. Fry, C. J. Keane, J. A. Koch, D. L. Matthews, S. Maxon, S. Mrowka, A. L. Osterheld, J. H. Scofield, and G. Shimkaveg, Inst. Phys. Conf. Ser. No. **116**, 221 (1990) (ed. G. J. Tallents).

[6] G. Jamelot, A. Klisnick, A. Carillon, H. Guennou, A. Sureau, and P. Jaeglé, J. Phys. B **18**, 4647 (1985).

[7] Z. Xu, P. Fan, L. Lin, Y. Li, X. Wang, P. Lu, R. Li, S. Han, L. Sun, A. Qian, B. Shen, Z. Jiang, Z. Zhang, and J. Zhou, Appl. Phys. Lett. **63**, 1023 (1993).

[8] Z. Z. Xu, P. Z. Fan, L. H. Lin, Y. L. Li, X. F. Wang, R. X. Li, P. X. Lu, S. S. Han, L. Sun, A. D. Qian, Z. Q. Zhang, and J. Z. Zhou, Phys. Rev. A **49**, 485 (1994).

[9] P. Zeitoun *et al.* (unpublished).

[10] G. J. Tallents, Opt. Commun. **37**, 108 (1981).

[11] P. Zeitoun, G. Jamelot, A. Carillon, P. Goedtkindt, H. Guennou, P. Jaeglé, A. Klisnick, C. Möller, B. Rus, and A. Sureau, AIP Conf. Proc. **332**, 55 (1994).

[12] A. H. Gabriel, Mon. Not. R. Astron. Soc. **160**, 99 (1972).

[13] A. H. Gabriel and T. M. Paget, J. Phys. B **5**, 673 (1972).

[14] K. R. Karim and C. P. Bhalla, Phys. Rev. A **45**, 3932 (1992).

[15] J. Dubau, M. Loulergue, and L. Steenman-Clark, Mon. Not. R. Astron. Soc. **190**, 125 (1980).

[16] U. I. Safronova, M. S. Safronova, and R. Bruch, J. Phys. B **28**, 2803 (1995).

[17] G. R. Blumenthal, G. W. F. Drake, and Wallace H. Tucker, Astrophys. J. **172**, 205 (1972).

[18] D. Duston, J. E. Rogerson, J. Davis, and M. Blaha, Phys. Rev. A **28**, 2968 (1983).

[19] A. Forsman, A. Ng, and G. Xu, J. Phys. B **26**, 889 (1993).

[20] J. G. Lunney and J. F. Seely, Phys. Rev. Lett. **46**, 342 (1981).

[21] J. G. Lunney, Phys. Rev. A **40**, 467 (1985).

[22] H. Van Regemorter, Astrophys. J. **136**, 906 (1962).

[23] A. Pradhan, D. W. Norcross, and D. G. Hummer, Astrophys. J. **246**, 1031 (1981).

[24] R. E. H. Clark, N. H. Magee, J. B. Mann, and A. L. Merts, Astrophys. J. **254**, 412 (1982).

[25] V. L. Jacobs and M. Blaha, Phys. Rev. A **21**, 525 (1980).
[26] J. Suleiman, H. G. Berry, R. W. Dunford, R. D. Deslattes, and P. Indelicato, Phys. Rev. A **49**, 156 (1994).
[27] G. A. Doschek, J. F. Meekins, R. W. Kreplin, T. A. Chubb, and H. Friedman, Astrophys. J. **164**, 165 (1971).
[28] F. Bombarda, R. Giannella, E. Källne, G. J. Tallents, F. Bely-Dubau, P. Faucher, M. Cornille, J. Dubau, and A. H. Gabriel, Phys. Rev. A **37**, 504 (1988).
[29] U. Feldman, G. A. Doscheck, D. J. Nagel, R. D. Cowan, and R. R. Whitlock, Astrophys. J. **192**, 213 (1974).
[30] K. L. Wong, P. Beiserdorfer, M. H. Chen, R. E. Mars, K. J. Reed, J. H. Scofield, D. A. Vogel, and R. Zasadzinski, Phys. Rev. A **48**, 2850 (1993).
[31] K. L. Wong, P. Beiserdorfer, K. J. Reed, and D. A. Vogel, Phys. Rev. A **51**, 1214 (1995).
[32] F. Bely-Dubau, P. Faucher, L. Steenman-Clark, M. Bitter, S. von Goeler, K. W. Hill, C. Camhy-Val, and J. Dubau, Phys. Rev. A **26**, 3459 (1982).
[33] M. Bitter, K. W. Hill, M. Zarnstorff, S. von Goeler, R. Hulse, L. C. Johnson, N. R. Sauthoff, S. Sesnic, K. M. Young, M. Tavernier, F. Bely-Dubau, P. Faucher, M. Cornille, and J. Dubau, Phys. Rev. A **32**, 3011 (1985).
[34] H. Baumhacker, G. Brederlow, E. Fill, Ch. Schrödter, R. Volk, S. Witkowski, K. J. Witte, Laser Particle Beams **11**, 353 (1993).
[35] R. W. Lee, B. L. Whitten, and R. E. Stout, J. Quant. Spectrosc. Radiat. Transfer. **32**, 91 (1984).
[36] I. H. Hutchinson, *Principles of Plasma Diagnostics* (Cambridge University Press, Cambridge, 1987), p. 199.
[37] F. Bely-Dubau, J. Dubau, P. Faucher, A. H. Gabriel, M. Loulergue, L. Steenman-Clark, S. Volonté, E. Antonicci, and C. G. Rapley, Mon. Not. R. Astron. Soc. **201**, 1155 (1982).
[38] G. J. Pert, J. Fluid. Mech. **131**, 401 (1983).
[39] R. W. P. McWhirter, in *Plasma Diagnostic Techniques*, edited by R. H. Huddlestone and Stanley L. Leonard (Academic Press, New York, 1965), p. 234.
[40] W. Brunner and R. W. John, Laser and Particles Beams **9**, 817 (1991).
[41] C. Popovics, C. Fievet, J. P. Geindreand, and J. C. Gauthier, Phys. Rev. A **40**, 3194 (1989).
[42] G. J. Tallents, M. H. Key, P. Norreys, J. Jacoby, R. Kodama, H. Baldis, J. Dunn, and D. Brown, Opt. Commun. **89**, 410 (1992).
[43] Y. Al-Hadithi, G. J. Tallents, J. Zhang, M. H. Key, P. A. Norreys, and R. Kodama, Phys. Plasmas **1**, 1279 (1994).